BJR

https://doi.org/10.1259/bjr.20200869

Received: 16 July 2020 | Revised: 04 February 2021 | Accepted: 10 February 2021

Cite this article as:
Sartoretti T, Sartoretti E, Wyss M, Mannil M, van Smoorenburg L, Eichenberger B, et al. Diffusion-weighted MRI of ischemic stroke at 3T: Value of synthetic *b*-values. *Br J Radiol* 2021; **94**: 20200869.

FULL PAPER

Diffusion-weighted MRI of ischemic stroke at 3T: Value of synthetic *b*-values

[1,2,3]THOMAS SARTORETTI, BMed, [1,2]ELISABETH SARTORETTI, cand med, [1,4]MICHAEL WYSS, BSc, [5]MANOJ MANNIL, MD, MSc, [1]LUUK VAN SMOORENBURG, BSc, [1]BARBARA EICHENBERGER, RT, [6,7]CAROLIN REISCHAUER, PhD, [8]ALEX ALFIERI, MD, [1]CHRISTOPH BINKERT, MD and [1]SABINE SARTORETTI-SCHEFER, MD

[1]Institute of Radiology, Kantonsspital Winterthur, Winterthur, Switzerland
[2]Faculty of Medicine, University of Zürich, Zürich, Switzerland
[3]Cardiovascular Research Institute Maastricht (CARIM), Maastricht University, Maastricht, the Netherlands
[4]Philips Healthsystems, Zürich, Switzerland
[5]Institute of Neuroradiology, Kantonsspital Aarau, Aarau, Switzerland
[6]Department of Medicine, University of Fribourg, Fribourg, Switzerland
[7]Department of Radiology, HFR Fribourg-Hôpital Cantonal, Fribourg, Switzerland
[8]Department of Neurosurgery, Kantonsspital Winterthur, Winterthur, Switzerland

Address correspondence to: Dr Sabine Sartoretti-Schefer
E-mail: *sabine.sartoretti@ksw.ch*

The authors Thomas Sartoretti and Elisabeth Sartoretti contributed equally to the work.

Objectives: Diffusion-weighted imaging (DWI) plays a crucial role in the diagnosis of ischemic stroke. We assessed the value of computed and acquired high b-value DWI in comparison with conventional b = 1000 s mm^{-2} DWI for ischemic stroke at 3T.

Methods: We included 36 patients with acute ischemic stroke who presented with diffusion abnormalities on DWI performed within 24 h of symptom onset. B-values of 0, 500, 1000 and 2000 s mm^{-2} were acquired. Synthetic images with b-values of 1000, 1500, 2000 and 2500 s mm^{-2} were computed. Two readers compared synthetic (syn) and acquired (acq) b = 2000 s mm^{-2} images with acquired b = 1000 s mm^{-2} images in terms of lesion detection rate, image quality, presence of uncertain hyperintensities and lesion conspicuity. Readers also selected their preferred b-value. Contrast ratio (CR) measurements were performed. Non-parametrical statistical tests and weighted Cohens' κ tests were computed.

Results: Syn1000 and syn1500 matched acq1000 images in terms of lesion detection rate, image quality and presence of uncertain hyperintensities but presented with significantly improved lesion conspicuity (p < 0.01) and were frequently selected as preferred b-values. Acq2000 images exhibited a similar lesion detection rate and improved lesion conspicuity (p < 0.01) but worse image quality (p < 0.01) than acq1000 images. Syn2000 and syn2500 images performed significantly worse (p < 0.01) than acq1000 images in most or all categories. CR significantly increased with increasing b-values.

Conclusion: Synthetic images at b = 1000 and 1500 s mm^{-2} and acquired DWI images at b = 2000 s mm^{-2} may be of clinical value due to improved lesion conspicuity.

Advances in knowledge: Synthetic b-values enable improved lesion conspicuity for DWI of ischemic stroke.

INTRODUCTION

For patients with ischemic stroke, an early and accurate diagnosis is essential in terms of achieving a favorable outcome.[1] Magnetic resonance imaging (MRI) plays a crucial role in enabling early diagnosis of ischemic stroke. Specifically, diffusion-weighted imaging (DWI) is considered the reference standard for early, accurate and reliable detection of ischemia.[1–3] DWI measures the random movement of water molecules[4] whereby the signal loss relative to non-DWIs is measured as a function of the so-called b-value. While for DWI of ischemic stroke, a b-value of around 1000 s/mm^2 is considered the reference standard,[1–3,5] select studies have explored the value of higher b-values.[1,2,5] Optimally, structures with a high degree of water signal and diffusion restriction are visualized more clearly on high b-value images.[6–8] Thus, it has been shown that high b-value imaging of ischemic stroke enables improved lesion conspicuity and detection of very small ischemic lesions.[1] Unfortunately, image quality and signal-to-noise ratio (SNR) deteriorate with increasing b-values. Moreover, the

increase in scan time to produce high b-value images (as compared to simply acquiring lower b-values) has to be considered.[6] Thus while potentially favorable, high b-value imaging of ischemic stroke has not gained a wider acceptance.

Computed DW images (cDWI) are synthetic DW images that can be calculated from acquired DW images with arbitrarily chosen b-values using voxelwise fitting. Synthetic images with high b-values exhibit stronger diffusion effects at a higher SNR than acquired images and they can be generated without additional scan time.[6,9,10] Thus cDWI has been shown to enable improved lesion conspicuity in comparison to acquired DWI in various body regions[11–13] such as the prostate,[14–17] breast[6,18,19] or the pancreas.[7]

Therefore, both acquired high b-value DW images and synthetic DW images may improve DW imaging of ischemic stroke. While the value of high b-value imaging for ischemic stroke has been investigated previously, to the best of our knowledge, cDWI has not been applied for brain imaging in the context of ischemic stroke. Thus in this study we reevaluated the utility of acquired high b-value images (b = 2000 s mm^{-2}) and evaluated the utility of synthetic images at four different b-values (b = 1000, 1500, 2000, 2500 s mm^{-2}) in comparison to acquired DW images at b = 1000 s mm^{-2}.

METHODS

This study was approved by the Cantonal Ethical Committee Zürich, Switzerland with general written informed consent from all patients.

Patients

In this retrospective analysis of a prospectively planned cohort study performed between January 2020 and March 2020, we assessed 94 consecutive patients who were referred to our tertiary radiology department due to clinically suspected acute ischemic stroke and/or transient ischemic attack (TIA). Initial assessment of all patients was performed by CT, CT-angiography and perfusion-weighted CT, followed by an MRI examination within 24 h of initial symptomatology.[1] We excluded patients who (a) did not complete the whole MR examination within 24 h of symptom onset and/or (b) presented with hemorrhagic infarctions (one patient), neoplasm (five patients) or other intracranial diseases (cytotoxic splenial lesion in one patient, postictal changes in one patient). 50 patients did not present with any diffusion abnormality. 36 patients (24 males and 12 females with a mean age of 76.6 years and age range of 53–93 years) were finally included in the study after applying exclusion criteria.

MRI and postprocessing

MR imaging was performed on a 3T scanner (Achieva, Philips Healthcare, Best, the Netherlands) with an eight-channel receive-only head coil array. As part of the clinical protocol the following sequences were acquired: 3D Turbo Spin Echo (TSE) Fluid Attenuated Inversion Recovery (FLAIR), 3D T1w Turbo Field Echo (TFE), Susceptibility-Weighted Imaging (SWI), 3D T2w TSE and Single Shot Spin Echo-Echo Planar Imaging DWI (SShot SE-EPI DWI) with b-values of 0, 500, 1000 and additionally (acquired separately) 2000 s mm^{-2} along three orthogonal gradient directions.[20] Parameters of the DWI sequence are shown in Table 1. As described in detail elsewhere,[6,9] synthetic images were generated by a mono-exponential decay model using dedicated vendor software.[6,9] Specifically, the software requires at least two lower acquired b-values to compute a particular synthetic image.[9] Synthetic images with b-values of 1500, 2000 and 2500 s mm^{-2} were computed from three lower acquired b-values (0, 500, 1000 s mm^{-2}).[14] Synthetic b = 1000 s mm^{-2} images were computed with two lower acquired b-values (0, 500 s mm^{-2}).[12] It should be mentioned that one should not calculate arbitrarily high b-values based on two or three lower acquired b-values, since fitting would deviate on very high b-values from the true signal decay curve due to kurtosis effects. Specifically, to calculate high b-values above b = 2500 s mm^{-2} one of the input values should be greater than b = 2000 s mm^{-2}.

Table 1. DWI sequence parameters

	SShot SE-EPI DWI b0, b500, b1000	SShot SE-EPI DWI b2000
Field of View (FoV)	240 × 240 x 165 mm^3	240 × 240 x 165 mm^3
Acquired voxel size	1.55 × 1.95 x 3.0 mm^3	1.55 × 1.95 x 3.0 mm^3
Reconstructed voxel size	0.9 × 0.9 x 3.0 mm^3	0.9 × 0.9 x 3.0 mm^3
Number of slices	50	50
Repetition time (TR)	6169 ms	6793 ms
Echo time (TE)	83 ms	90 ms
Flip angle	90°	90°
EPI factor	59	59
SENSE factor	P reduction = 2	P reduction = 2
Number of signal averages (NSA)	b0 = 1, b500 = 2, b1000 = 5	b2000 = 5
Receiver bandwidth	20.8 Hz/pixel	20.8 Hz/pixel
Acquisition time (mm:ss)	02:28	01:48
Calculated b values	b1000, b1500, b2000, b2500	–

However, images beyond $b = 2500\,s\,mm^{-2}$ will present with high levels of susceptibility related artifacts and noise,[1,2,21] which may considerably impair diagnostic readability. Thus, based on these considerations, we set a limit at synthetic $b = 2500\,s\,mm^{-2}$ images. Finally, concerning the choice of model, we employed a widely used mono-exponential decay model. However, it should be noted that for brain imaging more complex models may render more accurate results for the computation of synthetic images. To further investigate the impact of the choice of model on the image impression of synthetic images, we performed experimental tests on a subset of patients. The results from these tests are described in detail in the Supplementary Material 1.

Qualitative analysis

All qualitative analyses were performed by two readers in a blinded and randomized manner (S.S, board-certified neuroradiologist with 30 years of experience named reader one and T.S, trainee with 3 years of experience in medical imaging named reader 2). Images were reviewed on the PACS and readers were able to change windowing as necessary.[22]

Lesion detection, Presence of Uncertain Hyperintensities and Image Quality

For each patient, the readers evaluated image sets consisting of DW images (*i.e.* six image sets per patient, one set for each b-value), ADC map and FLAIR images[1,3,7] in a blinded and randomized manner. Specifically, the image sets from a single patient did not necessarily appear in sequential order. Readers were asked to search for the presence of areas with diffusion restriction as occurring in patients with acute or hyperacute stroke.[1] The readers were instructed to record the number, extent and location of lesions in each case.[1] Lesion extent was classified in four groups: punctate with up to 5 mm (Group 1), 6–10 mm (Group 2), 11–16 mm (Group 3) and larger than 16 mm (Group 4) in the widest extent on a single image slice. Furthermore, readers were asked to evaluate DW images firstly for the presence of uncertain hyperintensities on a 4-point Likert scale (1: multiple; 2: several; 3: a few; 4: none)[23] and secondly for image quality (*i.e.* visualization of anatomical structures, susceptibility and motion artefacts and image coarseness) using a 5-point Likert scale (1: non-diagnostic, 2: poor, 3: moderate, 4: good, 5: excellent). The category presence of uncertain hyperintensities was adapted from Byeon et al[23] and refers to the occurrence of small specks of hyperintensity on the b-value images that are most likely not caused by diffusion restriction but rather occur due to imperfections of the image acquisition or the voxelwise fitting (as in the case of synthetic images).

Lesion conspicuity

In a second step, one reader (S.S) first marked all lesions with small arrows on all b-value images for subsequent lesion conspicuity rating. If lesions were not visible on all images, they were excluded from the rating process. Lesion conspicuity was rated with a 3-point Likert scale (1: worse, 2: comparable, 3: better) relative to the acq1000 images. The readers rated every lesion and for subsequent statistical analysis, scores were averaged for each patient. The rating process was conducted as proposed elsewhere[24,25]; In brief, the two b-value images were presented to the readers in a 2-column format with the left-right order randomized as either acq1000 or acq2000/synthetic image. Each time the readers recorded whether they preferred the left or right image (or whether lesion conspicuity was similar) and after the rating session their scores were converted to the 3-point Likert scale by a further investigator (E.S). The images from a single patient did not necessarily appear in sequential order.

Preferred b-value

Finally, image sets consisting of all b-value images were generated for each patient. The b-value images were presented in a 6-column format in random order and readers were blinded to sequence and patient information. For each set, the readers were asked to choose their subjectively preferred b-value image.[6]

Quantitative analysis

For each patient, an image set consisting of six coregistered b-value images was created. In each case, the slice on which the largest lesion presented with the largest diameter was selected to generate a single image for each b-value.[6] One reader (T.S) then placed manually defined 2D ROIs into the lesion and into the normal contralateral brain tissue. ROI placement was checked by a second reader (**).[26] To ensure consistency of ROI size and position, ROIs were copied from the first image to the other images. From these ROIs, the signal intensities (SI) of infarct region ($SI_{infarct}$) and normal contralateral brain tissue (SI_{brain}) were derived for each patient and each b-value image.[1] Mean SI values were then used to calculate the contrast ratio (CR)[7] with the following formula:

$$CR = \frac{\left(SI_{infarct} - SI_{brain}\right)}{\left(SI_{infarct} + SI_{brain}\right)} \quad (1)$$

Statistical analysis

Scores from reader 1 (S.S) were considered the representative values for statistical analysis (*i.e.* in the categories image quality, presence of uncertain hyperintensities and lesion conspicuity) due to reader one being the most experienced.[27] Data were initially checked for normality and sphericity with QQ-Plots, Shapiro-Wilks tests and Mauchly tests. Scores from CR measurements, image quality and presence of uncertain hyperintensities were compared with Friedman tests and Nemenyi post-hoc tests for pairwise comparisons. Scores from lesion conspicuity ratings were assessed with exact binomial tests to test the null hypothesis that the probability for better results (ratings: 3) was equal to the probability for worse results (ratings: 1).[27] Spearman's rank correlation coefficients were computed to define the relationship between lesion size and lesion conspicuity rating scores for each b-value. Lesion detection rate and scores from "preferred b-values" were expressed with descriptive statistics. To assess interreader agreement, weighted Cohen's κ tests were computed. κ values were interpreted as follows: κ = 0.00–0.20, poor agreement; κ = 0.21–0.40, fair agreement; κ = 0.41–0.60, moderate agreement; κ = 0.61–0.80, good agreement and κ = 0.81–1.00, very good agreement.[7] Wherever appropriate, *p*-values were adjusted for multiple comparisons with the Benjamini-Hochberg procedure. p values < 0.05 were considered significant. Unless indicated otherwise, data are presented as median, [interquartile

Figure 1. Acute focal ovaloid ischemic infarct with diffusion abnormality of 9 mm maximal diameter in the posterior limb of the internal capsule along the corticospinal tract on the right side. The lesion is visible on all DW images, however the lesion (red arrows) conspicuity is increased on acq2000, syn1000, syn1500, syn2000 and syn2500 in comparison with the acq1000 image. The subjective image quality is reduced on the acq2000 image and on the syn2500 image.

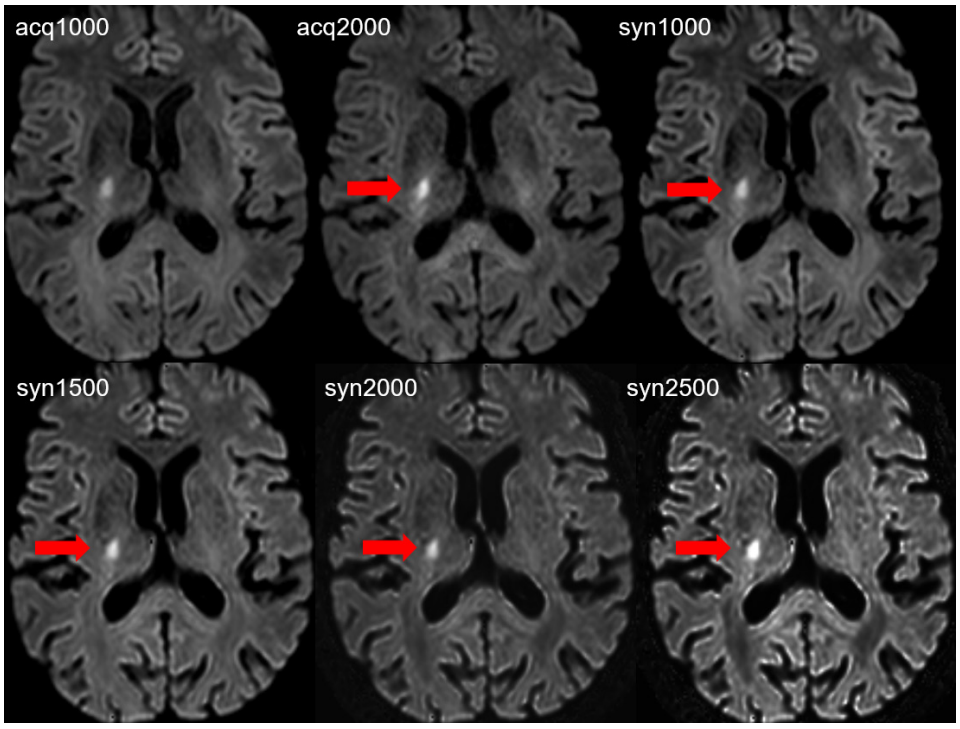

range]. All analyses were performed in the R programming language (v.3.6.3) (R Core Team, 2020) using the packages "PMCMR" to perform post-hoc tests, "irr" to compute tests for interreader agreement and "ggplot2" to generate figures.

RESULTS

Interesting image examples are provided as Figures 1 and 2.

Lesion detection

Reader 1 identified 139 lesions on the acq1000, syn1000 and syn1500 and acq2000 images, 124 lesions on syn2000 images and 122 lesions on syn2500 images. Reader two identified the same lesions on the acq1000, syn1000, syn1500 and acq2000 images, but identified 126 lesions on syn2000 images and 125 lesions on syn2500. Of the 139 lesions detected on acq1000, syn1000, syn1500 and acq2000 images, 82 were punctate (Group 1) and 57 presented with a diameter between 5 and 73 mm (Groups 2, 3 and 4). Lesions that were not detected on syn2000, and syn2500 images were all punctate.

Presence of uncertain hyperintensities

Syn2000 [3, (3, 3), $p < 0.01$] and syn2500 [3, (2, 3), $p < 0.001$] images were found to exhibit significantly more uncertain hyperintensities as compared with acq1000 [4, (3.75, 4)], acq2000 [4, (3, 4)], syn1000 [4, (3, 4)] and syn1500 [4, (3, 4)] images. Interreader agreement ranged from good to very good (κ = 0.742–0.941). The data are presented in Figure 3.

Image quality

Image quality was rated similarly well on acq1000 [4, (4, 4)], syn1000 [5, (4, 5)] and syn1500 [4.5, (4, 5)] images with a tendency towards improved scores on syn1000 and syn1500 images. However, acq2000 [3, (3, 4), $p < 0.001$], syn2000 [3, (3, 3), $p < 0.001$] and syn2500 [3, (2, 3), $p < 0.001$] images were found to exhibit significantly worse image quality than acq1000 images. Between acq2000, syn2000, syn2500 images, there were no significant differences in image quality. Interreader agreement ranged from moderate to very good (κ = 0.482–0.86). The data are presented in Figure 3.

Lesion conspicuity

The data are presented in Figures 3 and 4 and a detailed overview is given in Table 2. 121 lesions were rated. Lesion conspicuity was rated significantly better on syn1000 (2, [2, 2.5], $p < 0.001$), syn1500 [2.5, (2, 2.95), $p < 0.001$] and acq2000 [2.1, (2, 2.6), $p < 0.001$] images than on acq1000 images. On syn2000 images [2, (1.6, 2.2), $p = 0.67$], lesion conspicuity was considered comparable and on syn2500 images [1.9, (1.5, 2), $p = 0.001$] worse than on acq1000 images. Only on syn1000 images, a significant inverse relationship between lesion conspicuity scores and lesion extent was observed ($\rho = -0.33$, $p < 0.01$). Interreader agreement ranged from moderate to good (κ = 0.42–0.69).

Preferred b-value

The data are presented visually with a radarchart (Figure 5). In brief, both readers chose syn1500 images most often as their

Figure 2. Three punctate acute ischemic infarcts, two lesions in the postcentral gyrus (medial and lateral) and one lesion in the lateral part of the precuneus are depicted on the left hemisphere. The acute infarct in the medial postcentral gyrus (red arrow) shows better lesion conspicuity on the acq2000 and the syn1000, syn1500, syn2000 and syn2500 images compared to the acq1000 image. The lesion conspicuity of the acute infarcts in the lateral part of the postcentral gyrus and in the precuneus is comparable on acq1000, acq2000 (yellow arrows) and syn1000 image (yellow arrow), but slightly reduced on syn1500 (yellow arrows with white border) images. The lesion (white arrows) is not reliably identified on syn2000 and syn2500 due to similar appearance of hyperintensities of uncertain origin (green arrows) in the normal cortex thus also resulting in reduced lesion conspicuity.

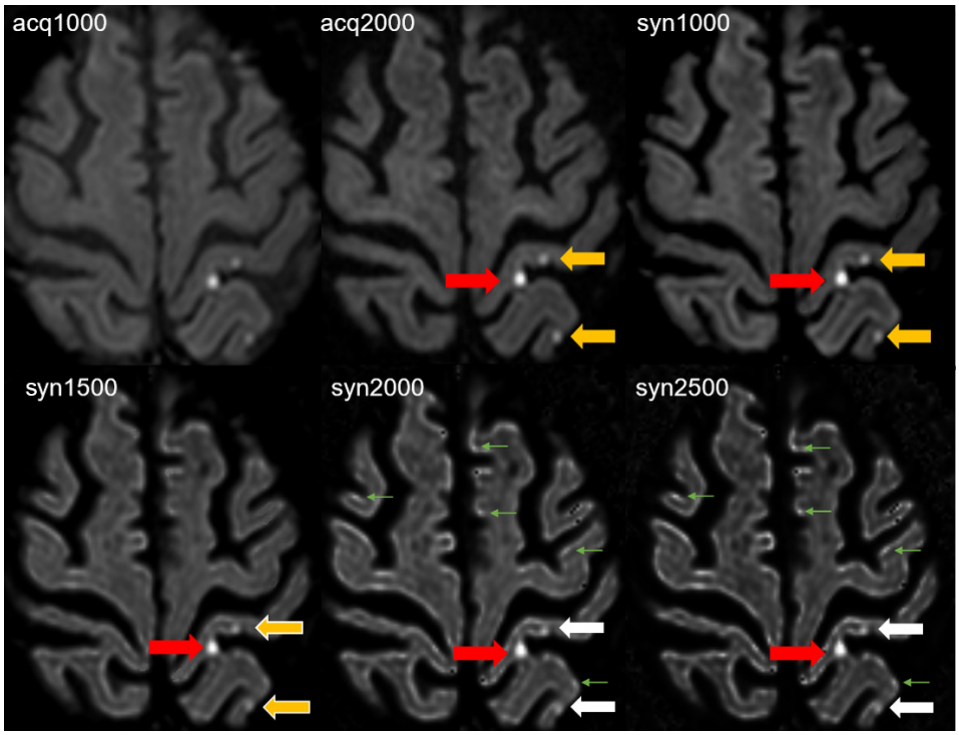

preferred b-value (reader 1: 15 times, reader 2: 17 times) followed by syn1000 images (reader 1: nine times, reader 2: 10 times). Acq1000 (reader 1: four times, reader 2: four times), acq2000 (reader 1: two times, reader 2: two times) and syn2000 (reader 1: six times, reader 2: three times) images were chosen less frequently. Syn2500 images were never chosen as the preferred b-value. Interreader agreement was very good ($\kappa = 0.86$).

Contrast Ratio (CR)

As expected, CR increased with increasing b-values. Acq2000 [0.38, (0.3, 0.53), $p < 0.01$], syn1500 [0.42, (0.29, 0.53), $p < 0.01$], syn2000 [0.48, (0.3, 0.58), $p < 0.001$] and syn2500 [0.56, (0.34, 0.64), $p < 0.001$] images all exhibited significantly improved CR compared to acq1000 [0.32, (0.24, 0.43)] and syn1000 [0.31, (0.24, 0.43)] images. Furthermore, syn2500 images exhibited significantly higher CR values than the acq2000 ($p < 0.01$) and syn1500 images ($p < 0.01$). The data is visualized in Figure 3.

DISCUSSION

In this study, we evaluated the utility of acquired high b-value DW images and synthetic b-value DW images in comparison with conventional acquired DW images at $b = 1000\,s\ mm^{-2}$ for ischemic stroke imaging at 3T. We found that syn1000 and syn1500 images presented with comparable image quality, improved lesion conspicuity and a similar lesion detection rate as acq1000 images. The acq2000 images presented with a similar lesion detection rate and improved lesion conspicuity but diminished image quality in comparison with acq1000 images. Syn2000 images presented with a similar lesion conspicuity as acq1000 images, but performed worse in terms of lesion detection rate, image quality and presence of uncertain hyperintensities. Syn2500 images performed worse than acq1000 images in all rating categories (except for CR values).

Our results suggested that syn1000 and especially syn1500 images are superior to synthetic images with higher b-values are consistent with results from other studies. Bickel et al evaluated the utility of synthetic b-value images for breast imaging. Synthetic b-values ranging from $b = 1000$ to $b = 2000\,s\ mm^{-2}$ were compared to acquired $b = 850\,s\ mm^{-2}$ images. The authors concluded that image quality and lesion conspicuity was optimal on the synthetic images with b values of around $1500\,s\ mm^{-2}$.[6] Interestingly, both in the present study and the study of Bickel et al[6] the contrast between lesion and parenchyma increased steadily with increasing b-values, which can be expected as high b-values exhibit stronger diffusion effects. While this effect may offer theoretical benefits such as improved lesion visibility, it should be noted that the proper visualization of lesions does not solely depend on the raw signal intensity difference between lesion and surrounding parenchyma, which may explain discrepancies between subjective lesion conspicuity scores and quantitative CR measurements.

Figure 3. Boxplots depicting data from quantitative and qualitative image analysis from reader 1. The line in the box shows the median, the lower and upper hinges correspond to the first and third quartiles. The upper/lower whisker extends from the hinge to the largest/smallest value no further than 1.5 * IQR from the hinge. For contrast ratio (CR), violin plots showing the probability density of the data at specific values smoothed by a kernel density estimator surround the boxplots.

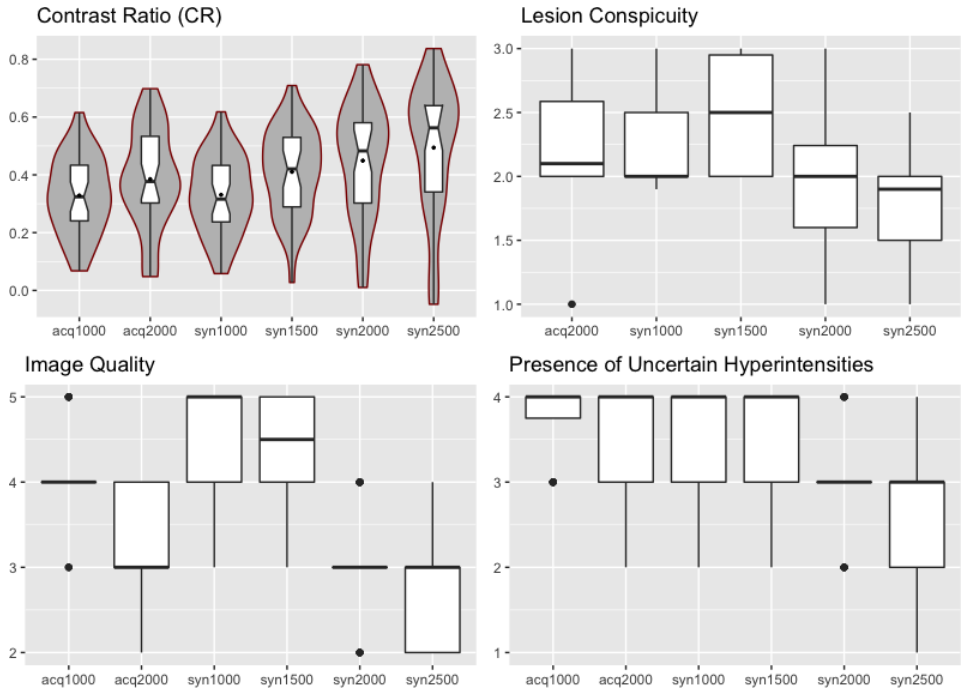

Similarly, Rosenkrantz et al[16] evaluated synthetic images ranging from $b = 1000$ to $b = 5000$ s mm^{-2} for prostate imaging. Synthetic images of $b = 1500$ s mm^{-2} were found to outperform images exceeding b-values of 2500 s/mm^2. However, synthetic $b = 1000$ s mm^{-2} images were also described as non-optimal.

Concerning the value of acquired high b-values images for stroke imaging, our results are similar to those from previous studies such as Cihangiroglu et al[1] as our acq2000 images presented with better lesion conspicuity yet lower image quality.

Furthermore, it has been shown that high b-values are useful to detect additional small lesions, especially in patients presenting with hyperacute stroke that may not be visible on lower b-value images.[1,2,5] In the present study we did not encounter such a case possibly due to the study design (*i.e.* patients within 24 rather than for example only within 6 h of symptom onset were included). Nonetheless, the value of acquired high b-values is debatable, as it is questionable whether the longer scan time can be justified by the potentially slightly higher sensitivity towards very small lesions.

Hypothetically, synthetic high b-value images could provide a viable alternative in such situations. In our study, syn2000 and syn2500 suffered from reduced lesion detection rate presumably due to increased presence of uncertain hyperintensities. These hyperintensities are also visible on synthetic high b-value images provided by Kamata et al[11] who studied the utility of synthetic images in pediatric encephalopathy or Bickel et al[6] who investigated the use of synthetic images in breast imaging. These hyperintensities often appear at the border of the cortex and their intensity and number seem to increase with increasing b-values on synthetic images. The etiology of these hyperintensities is unknown. However, we suspect that, firstly, they are related to the voxelwise fitting procedure and partial volume effects affecting acquired images with low b-values (*i.e.* $b = 0$ s mm^{-2}) and, secondly, that they represent, to some extent, genuine biological processes. Unfortunately, these hyperintensities may appear similar to small ischemic lesions and thus small lesions may mistakenly be dismissed as a hyperintensity, which presumably occurred in this study thus leading to a reduced lesion detection rate. Therefore, syn2000 and syn2500 images cannot be considered true alternatives to acq2000 or even acq1000 images. Thus, to further address the sensitivity of high b-values towards small lesions in a hyperacute setting, we hypothesize that the increased sensitivity is only achievable with acquired high b-value images (*i.e.* acq2000 and beyond) and possibly also with syn1500 images as these synthetic images did not suffer a loss of lesion detection rate and did not exhibit increased presence of uncertain hyperintensities. This should however be addressed in future studies.

To improve reading experience of patient studies, especially the visualization of smaller lesions is of relevance. There was a significant inverse relationship for syn1000 between lesion extent and lesion conspicuity score with smaller lesions having higher lesion conspicuity scores. For the other b-value images, no significant association between lesion conspicuity scores and lesion extent was found, which shows that the occurrence of improved (or diminished) lesion conspicuity is irrespective of the extent of lesions and may occur equally likely for small as well as large

Figure 4. Relationship between lesion extent and lesion conspicuity scores for each b-value. The size of the black dots on the left side is proportional to the number of lesions of a given extent receiving a particular lesion conspicuity score. A smoothed regression line approximated with the LOESS function was added, whereby 95% confidence intervals are shown as grey zones. On the right side, stacked barplots show the distribution of lesion conspicuity scores for a given lesion extent.

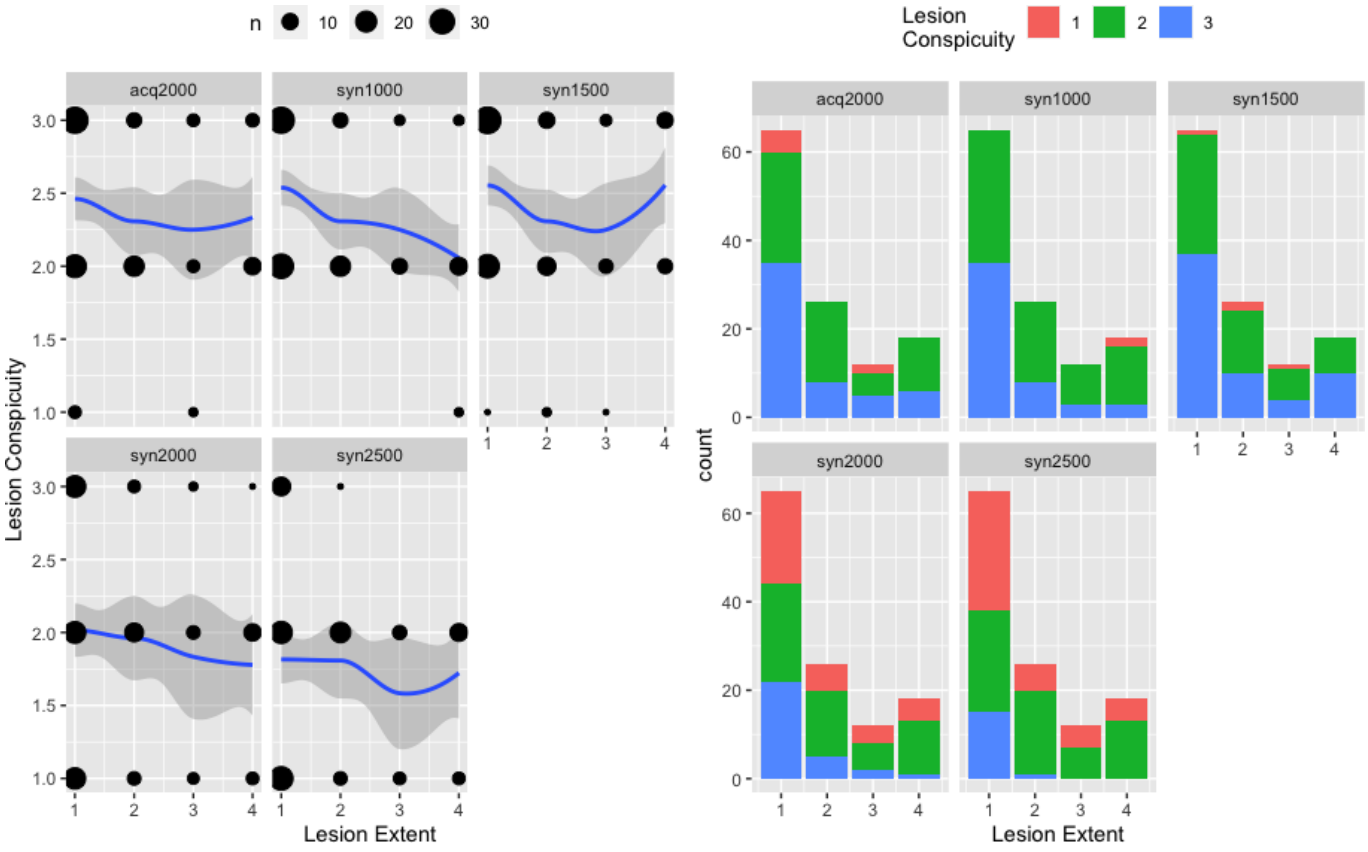

lesions. Thus for the visualization of small lesions, acq2000, syn1000 and syn1500 images are all equally well suited and may all enable improved visualization of small lesions as compared to acq1000 images.

Finally, the computation procedure for synthetic images has to be considered. For this study, synthetic images were generated by a mono-exponential decay model. Specifically, at least two lower acquired b-values are required to compute a higher, synthetic b-value image.[9] However, there are further models to fit the data, such as bi-exponential decay models. It has been suggested, that these models may be more suitable for DW imaging of the brain as the diffusion of water molecules is non-gaussian in brain tissues.[28–30] However, to achieve robustness, these models require many lower acquired b-values to generate computed images.[31] While feasible in research settings, there are certain limitations in terms of scantime in a clinical setting and acquiring several more lower b-values would have not been reasonable for patients. Furthermore, due to lack of standardization, bi-exponential models have not seen widespread clinical adoption yet.[31]

Moreover, it should be emphasized that we did not derive any quantitative parameters from the acquired or synthetic images but focused solely on assessing the images qualitatively. Thus, slight differences between the images of various models would

Table 2. Detailed overview of the data from lesion conspicuity ratings for both readers. Data from reader one were considered representative for statistical analysis

Nr. of cases per rating category (1, 2 or 3) with a total of 121 lesions	acq2000	syn1000	syn1500	syn2000	syn2500
Lesion Conspicuity worse than acq1000 (1)	Reader 1: 7 Reader 2: 8	Reader 1: 2 Reader 2: 3	Reader 1: 4 Reader 2: 5	Reader 1: 35 Reader 2: 22	Reader 1: 42 Reader 2: 34
Lesion Conspicuity comparable to acq1000 (2)	Reader 1: 60 Reader 2: 59	Reader 1: 70 Reader 2: 49	Reader 1: 55 Reader 2: 47	Reader 1: 56 Reader 2: 61	Reader 1: 63 Reader 2: 62
Lesion Conspicuity better than acq1000 (3)	Reader 1: 54 Reader 2: 54	Reader 1: 49 Reader 2: 69	Reader 1: 62 Reader 2: 69	Reader 1: 30 Reader 2: 38	Reader 1: 16 Reader 2: 25

Figure 5. Radar chart depicting the choice of preferred b-values for each reader.

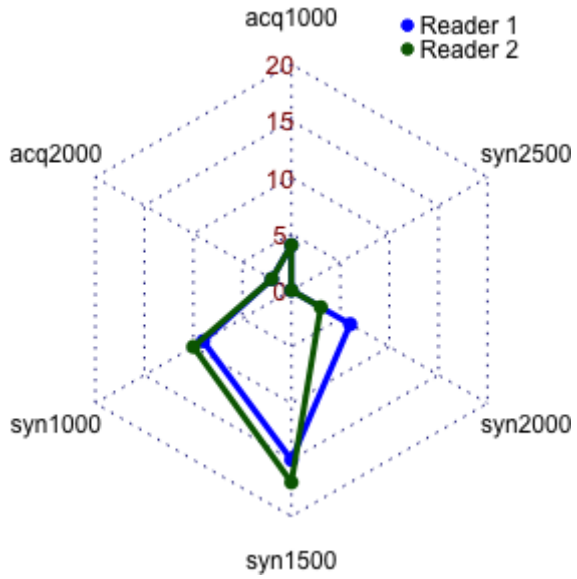

have presumably not been apparent, especially when considering that readers were allowed to adjust the windowing themselves.

Our study has several limitations: Firstly, while in range of similar studies,[1,11,32] the sample size is fairly limited, as many patients had to be excluded. Secondly, while in line with other studies,[6,13,14] we did not acquire DW images for every synthetic counterpart. This would have prolonged scan time considerably, which was not reasonable for patients in a clinical setting. Also, we only used three gradient direction DWI (as recommended elsewhere[20] and did not assess the influence of other DWI protocols (*i.e.* with more gradient directions). This limits the generalizability of our results. Thirdly, it should be mentioned that windowing may impact the perception of subjective image quality on synthetic DW images. Here, readers were allowed to change windowing as necessary, but scores could have differed considerably when windowing would have been fixed prior to the qualitative analyses. For institutions using fixed windowing settings for DWI interpretation, this should be considered. Finally, we could not assess the true diagnostic performance of the b-value images in terms of lesion detection, as this is generally only possible in an experimental setting. Thus, we resorted to comparing the synthetic images to the standard acq1000 images instead.

In conclusion, we show that synthetic b-value images at b = 1000 and 1500 s mm^{-2} offer advantages over conventional acquired b = 1000 s mm^{-2} images and may thus improve the reading experience of patient studies for neuroradiologists. Acquired b = 2000 s mm^{-2} images also enable improved lesion visualization but suffer from reduced image quality and additional scan time. Finally, synthetic images at b = 2000 and b = 2500 s mm^{-2} cannot be considered viable alternatives to acquired DW images due to reduced lesion detection rates.

We, therefore, recommend computing synthetic images at b-values of 1000 and 1500 s mm^{-2} images in addition to conventional acquired b = 1000 s mm^{-2} images as they may offer improved lesion visualization (which is especially useful for small lesions) and thus reading reliability. In contrast to additionally acquiring b = 2000 images, which may also offer improved lesion visualization, scan time is not prolonged by using synthetic b = 1000 and b = 1500 s mm^{-2} images.

CONTRIBUTORS

TS, ES, SS, MW, MM, AA and CB designed the study and interpreted the results. MW, LVS, and BE performed the experiments. TS analyzed the data. TS, SS, MW and ES wrote the paper. CR provided technical advice. All coauthors contributed constructively to the manuscript.

FUNDING

No funding was received for this study.

DATA STATEMENT

Data is available upon enquiry to the corresponding author.

ETHICS APPROVAL

This study received institutional review board approval.

DISCLOSURE

Michael Wyss is a part time employee of Philips Healthcare Switzerland. The remaining authors declare that the research was conducted in the absence of any commercial or financial relationships that could be construed as a potential conflict of interest.

REFERENCES

1. Cihangiroglu M, Citci B, Kilickesmez O, Firat Z, Karlıkaya G, Uluğ AM, et al. The utility of high b-value DWI in evaluation of ischemic stroke at 3T. *Eur J Radiol* 2011; **78**: 75–81. doi: https://doi.org/10.1016/j.ejrad.2009.10.011
2. Lettau M, Laible M. 3-T high-b-value diffusion-weighted MR imaging in hyperacute ischemic stroke. *J Neuroradiol* 2013; **40**: 149–57. doi: https://doi.org/10.1016/j.neurad.2012.08.007
3. Seith F, Schmidt H, Nikolaou K, Ernemann U, Bier G. Voxelwise computed diffusion-weighted imaging for the detection of cytotoxic oedema in brain imaging: a pilot study. *Neuroradiol J* 2018; **31**: 518–22. doi: https://doi.org/10.1177/1971400918789382
4. Hu S, Zhang H, Wang X, Sun Z, Ge Y, Li J, et al. Can diffusion-weighted MR imaging be used as a tool to predict extrathyroidal extension in papillary thyroid carcinoma? *Acad Radiol* 2020; **375**. doi: https://doi.org/10.1016/j.acra.2020.03.005
5. Kim HJ, Choi CG, Lee DH, Lee JH, Kim SJ, Suh DC. High-b-value diffusion-weighted MR imaging of hyperacute ischemic stroke

at 1.5T. *AJNR Am J Neuroradiol* 2005; **26**: 208–15.
6. Bickel H, Polanec SH, Wengert G, Pinker K, Bogner W, Helbich TH, et al. Diffusion-weighted MRI of breast cancer: improved lesion visibility and image quality using synthetic b-Values. *J Magn Reson Imaging* 2019; **50**: 1754–61. doi: https://doi.org/10.1002/jmri.26809
7. Fukukura Y, Kumagae Y, Hakamada H, Shindo T, Takumi K, Kamimura K, et al. Computed diffusion-weighted MR imaging for visualization of pancreatic adenocarcinoma: comparison with acquired diffusion-weighted imaging. *Eur J Radiol* 2017; **95**: 39–45. doi: https://doi.org/10.1016/j.ejrad.2017.07.022
8. Dreher C, Kuder TA, König F, Paech D, Tavakoli A, Laun FB, et al. Advanced diffusion-weighted abdominal imaging: qualitative and quantitative comparison of high and ultra-high b-Values for lesion detection and image quality. *Invest Radiol* 2020; **55**: 285–92. doi: https://doi.org/10.1097/RLI.0000000000000639
9. Higaki T, Nakamura Y, Tatsugami F, Kaichi Y, Akagi M, Akiyama Y, et al. Introduction to the technical aspects of computed diffusion-weighted imaging for radiologists. *Radiographics* 2018; **38**: 1131–44. doi: https://doi.org/10.1148/rg.2018170115
10. Blackledge MD, Leach MO, Collins DJ, Koh D-M. Computed diffusion-weighted MR imaging may improve tumor detection. *Radiology* 2011; **261**: 573–81. doi: https://doi.org/10.1148/radiol.11101919
11. Kamata Y, Shinohara Y, Kuya K, Tsubouchi Y, Saito Y, Maegaki Y, et al. Computed diffusion-weighted imaging for acute pediatric encephalitis/encephalopathy. *Acta Radiol* 2019; **60**: 1341–7. doi: https://doi.org/10.1177/0284185118823335
12. Shimizu H, Isoda H, Fujimoto K, Kawahara S, Furuta A, Shibata T, et al. Comparison of acquired diffusion weighted imaging and computed diffusion weighted imaging for detection of hepatic metastases. *Eur J Radiol* 2013; **82**: 453–8. doi: https://doi.org/10.1016/j.ejrad.2012.10.020
13. Takeuchi M, Matsuzaki K, Harada M. Computed diffusion-weighted imaging for differentiating decidualized endometrioma from ovarian cancer. *Eur J Radiol* 2016; **85**: 1016–9. doi: https://doi.org/10.1016/j.ejrad.2016.03.009
14. Jendoubi S, Wagner M, Montagne S, Ezziane M, Mespoulet J, Comperat E, et al. MRI for prostate cancer: can computed high b-value DWI replace native acquisitions? *Eur Radiol* 2019; **29**: 5197–204. doi: https://doi.org/10.1007/s00330-019-06085-z
15. Maas MC, Fütterer JJ, Scheenen TWJ. Quantitative evaluation of computed high B value diffusion-weighted magnetic resonance imaging of the prostate. *Invest Radiol* 2013; **48**: 779–86. doi: https://doi.org/10.1097/RLI.0b013e31829705bb
16. Rosenkrantz AB, Parikh N, Kierans AS, Kong MX, Babb JS, Taneja SS, et al. Prostate cancer detection using computed very high b-value diffusion-weighted imaging: how high should we go? *Acad Radiol* 2016; **23**: 704–11. doi: https://doi.org/10.1016/j.acra.2016.02.003
17. Ueno Y, Takahashi S, Ohno Y, Kitajima K, Yui M, Kassai Y, et al. Computed diffusion-weighted MRI for prostate cancer detection: the influence of the combinations of b-values. *Br J Radiol* 2015; **88**: 20140738. doi: https://doi.org/10.1259/bjr.20140738
18. Park JH, Yun B, Jang M, et al. Comparison of the diagnostic performance of synthetic versus acquired high b-Value (1500 s/mm. *J Magn Reson Imaging* 2019; **49**: 857–63.
19. Cheng Q, Ye S, Fu C, Zhou J, He X, Miao H, et al. Quantitative evaluation of computed and voxelwise computed diffusion-weighted imaging in breast cancer. *Br J Radiol* 2019; **92**: 20180978. doi: https://doi.org/10.1259/bjr.20180978
20. Havsteen I, Ovesen C, Willer L, Nybing JD, Ægidius K, Marstrand J, et al. Comparison of 3- and 20-Gradient direction diffusion-weighted imaging in a clinical subacute cohort of patients with transient ischemic attack: application of standard vendor protocols for lesion detection and final infarct size projection. *Front Neurol* 2017; **8**: 691. doi: https://doi.org/10.3389/fneur.2017.00691
21. Burdette JH, Durden DD, Elster AD, Yen YF. High b-value diffusion-weighted MRI of normal brain. *J Comput Assist Tomogr* 2001; **25**: 515–9. doi: https://doi.org/10.1097/00004728-200107000-00002
22. Cauley KA, Thangasamy S, Dundamadappa SK. Improved image quality and detection of small cerebral infarctions with diffusion-tensor trace imaging. *AJR Am J Roentgenol* 2013; **200**: 1327–33. doi: https://doi.org/10.2214/AJR.12.9816
23. Byeon J, Kim JY, Cho A-H. Readout-segmented echo-planar imaging in diffusion-weighted MR imaging of acute infarction of the brainstem and posterior fossa: comparison of single-shot echo-planar diffusion-weighted sequences. *Clin Imaging* 2015; **39**: 765–9. doi: https://doi.org/10.1016/j.clinimag.2015.06.001
24. Li Z, Hu HH, Miller JH, Karis JP, Cornejo P, Wang D, et al. A spiral spin-echo MR imaging technique for improved flow artifact suppression in T1-weighted postcontrast brain imaging: a comparison with Cartesian turbo spin-echo. *AJNR Am J Neuroradiol* 2016; **37**: 642–7. doi: https://doi.org/10.3174/ajnr.A4600
25. Ooi MB, Li Z, Robison RK, Wang D, Anderson AG, Zwart NR, et al. Spiral T1 spin-echo for routine postcontrast brain MRI exams: a multicenter Multireader clinical evaluation. *AJNR Am J Neuroradiol* 2020; **41**: 238–45. doi: https://doi.org/10.3174/ajnr.A6409
26. Sartoretti T, Sartoretti E, Wyss M, Schwenk Árpád, van Smoorenburg L, Eichenberger B, et al. Compressed sense accelerated 3D T1w black blood turbo spin echo versus 2D T1w turbo spin echo sequence in pituitary magnetic resonance imaging. *Eur J Radiol* 2019; **120**: 108667. doi: https://doi.org/10.1016/j.ejrad.2019.108667
27. Sartoretti T, van Smoorenburg L, Sartoretti E, et al. Ultrafast intracranial vessel imaging with Non-Cartesian spiral 3-dimensional time-of-flight magnetic resonance angiography at 1.5 T: an in vitro and clinical study in healthy volunteers. *Invest Radiol* 2019; **55**: 293–303.
28. Mulkern RV, Haker SJ, Maier SE. On high B diffusion imaging in the human brain: ruminations and experimental insights. *Magn Reson Imaging* 2009; **27**: 1151–62. doi: https://doi.org/10.1016/j.mri.2009.05.003
29. Grinberg F, Farrher E, Kaffanke J, Oros-Peusquens A-M, Shah NJ. Non-Gaussian diffusion in human brain tissue at high b-factors as examined by a combined diffusion kurtosis and biexponential diffusion tensor analysis. *Neuroimage* 2011; **57**: 1087–102. doi: https://doi.org/10.1016/j.neuroimage.2011.04.050
30. Clark CA, Le Bihan D. Water diffusion compartmentation and anisotropy at high B values in the human brain. *Magn Reson Med* 2000; **44**: 852–9. doi: https://doi.org/10.1002/1522-2594(200012)44:6<852::AID-MRM5>3.0.CO;2-A
31. Malagi AV, Das CJ, Khare K, Calamante F, Mehndiratta A. Effect of combination and number of B values in IVIM analysis with post-processing methodology: simulation and clinical study. *MAGMA* 2019; **32**: 519–27. doi: https://doi.org/10.1007/s10334-019-00764-0
32. DelPriore MR, Biswas D, Hippe DS, Zecevic M, Parsian S, Scheel JR, et al. Breast cancer Conspicuity on computed versus acquired high b-Value diffusion-weighted MRI. *Acad Radiol* 2020;16 Apr 2020. doi: https://doi.org/10.1016/j.acra.2020.03.011